Supplementary Information

Mitigating Anisotropic Changes in Classical Layered Oxide Materials by Controlled Twin Boundary Defects for Long Cycle Life Li-ion Batteries

Hyeseung Chung,[1†] Yixuan Li,[1†] Minghao Zhang[1*], Antonin Grenier,[2] Carlos Mejia,[1] Diyi Cheng,[1] Baharak Sayahpour,[1] Chengyu Song,[3] Meghan Hannah Shen,[1] Ricky Huang,[1] Erik A. Wu,[1] Karena W. Chapman,[2] Suk Jun Kim[4*], Y. Shirley Meng[1,5*]

[1] Department of NanoEngineering, University of California San Diego, La Jolla, CA, USA.

[2] Department of Chemistry, Stony Brook University, Stony Brook, New York 11794, USA

[3] National Center for Electron Microscopy, Molecular Foundry, Lawrence Berkeley National Laboratory, Berkeley, CA 94720, USA

[4] School of Energy, Materials and Chemical Engineering, Korea University of Technology and Education, Cheonan, 31253, Republic of Korea

[5] Pritzker School of Molecular Engineering, The University of Chicago, Chicago, IL 60637, United States

[†] These authors contributed equally to the work

*Corresponding author

Email: shirleymeng@uchicago.edu, skim@koreatech.ac.kr, miz016@eng.ucsd.edu

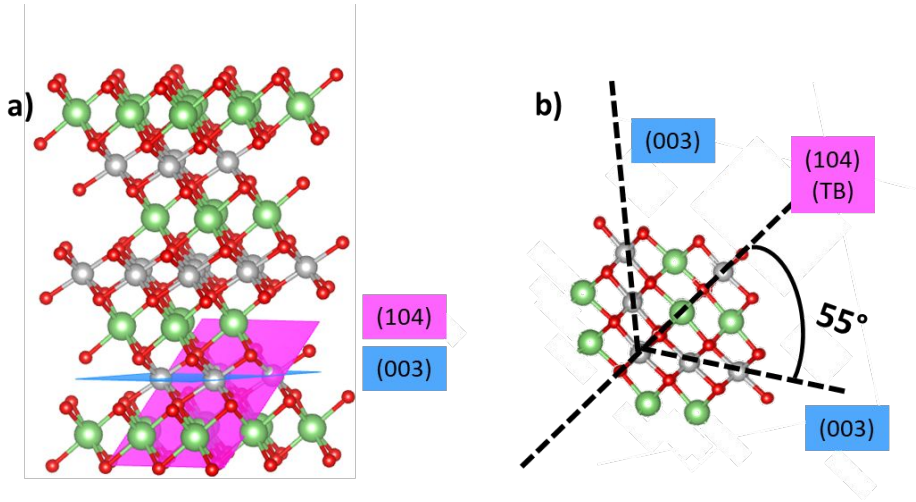

Figure S1. (a) Schematic of the (003) and (104) planes in a layered structure. (b) Schematic of the two (003) domains on the two sides of the (104) plane, forming the 110° angle between the two (003) planes.

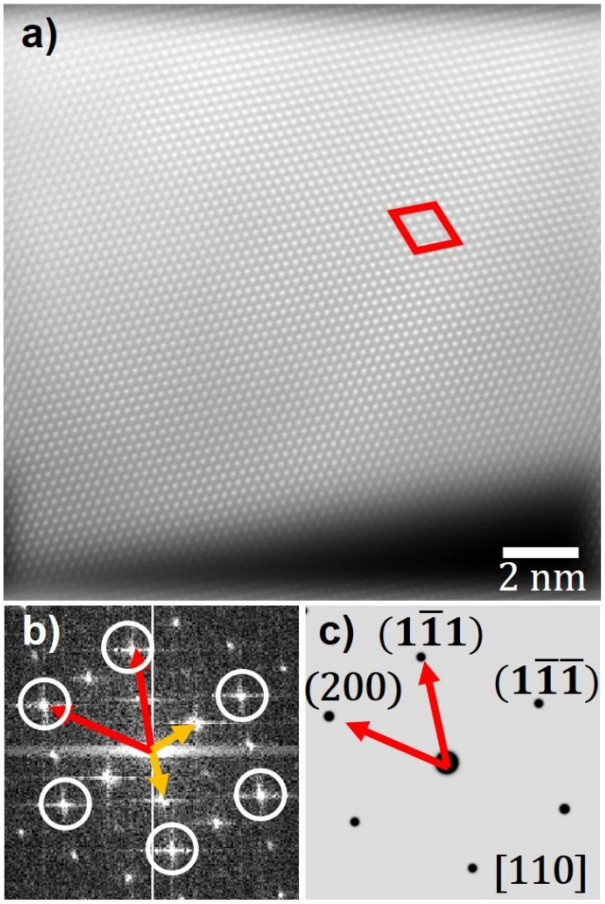

Figure S2. a) Fourier filtered image of Figure 2a, generated by applying periodic masks of the rock-salt phase. Atomic structure in the red box is similar to the one in the orange box on Figure 2f. b) FFT image of Figure 2a; the white circles are the periodic masks of the rock-salt phase applied to generate Figure S2a; the position of periodic masks is determined by two vectors indicated by the two red arrows which correspond to the (200) and $(11\bar{1})$ reciprocal vectors of NiO (that has a rock-salt structure). c) Simulated diffraction pattern of rock-salt NiO (with [110] zone axis); The red arrows show the (200) and $(11\bar{1})$ reciprocal vectors of NiO.

It should be noted that the periodic masks for Figure S2a are different from the ones used for Figure 2f. The periodic masks for Figure 2f are determined by two (003) vectors from the two domains divided by the twin boundary. These vectors are indicated by two orange arrows on Figure S2b.

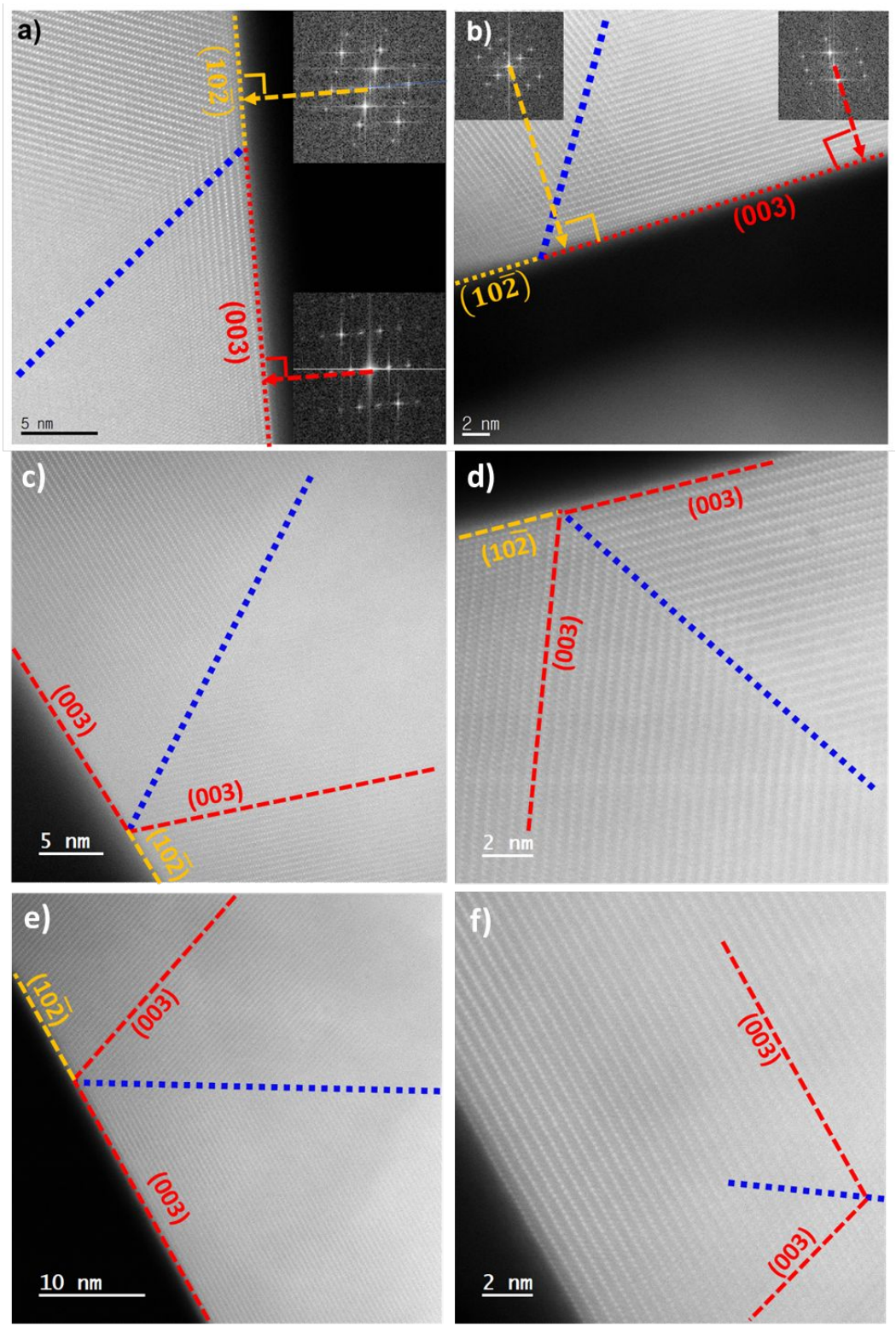

Figure S3. More STEM images of TB-NMC with the twin boundary marked with a blue line. a) and b) TB-NMC442, c)- f) TB-NMC622. The surfaces of the particles were terminated by (003) and $(\mathbf{10\bar{2}})$ planes.

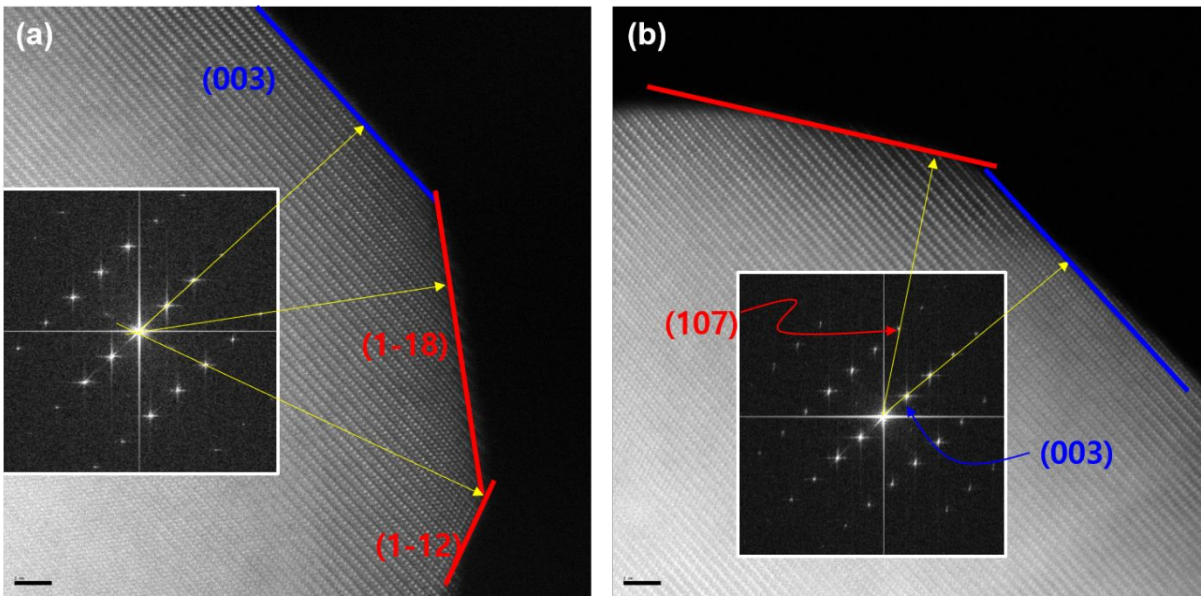

Figure S4. Two STEM images of areas without a twin boundary in TB-NMC442. The insets show the FFT images of the particles. The FFT patterns confirm that surfaces of the particles were terminated by (a) (003), $(1\bar{1}8)$, **and** $(1\bar{1}2)$ planes and (b) (003) and **(107)** planes.

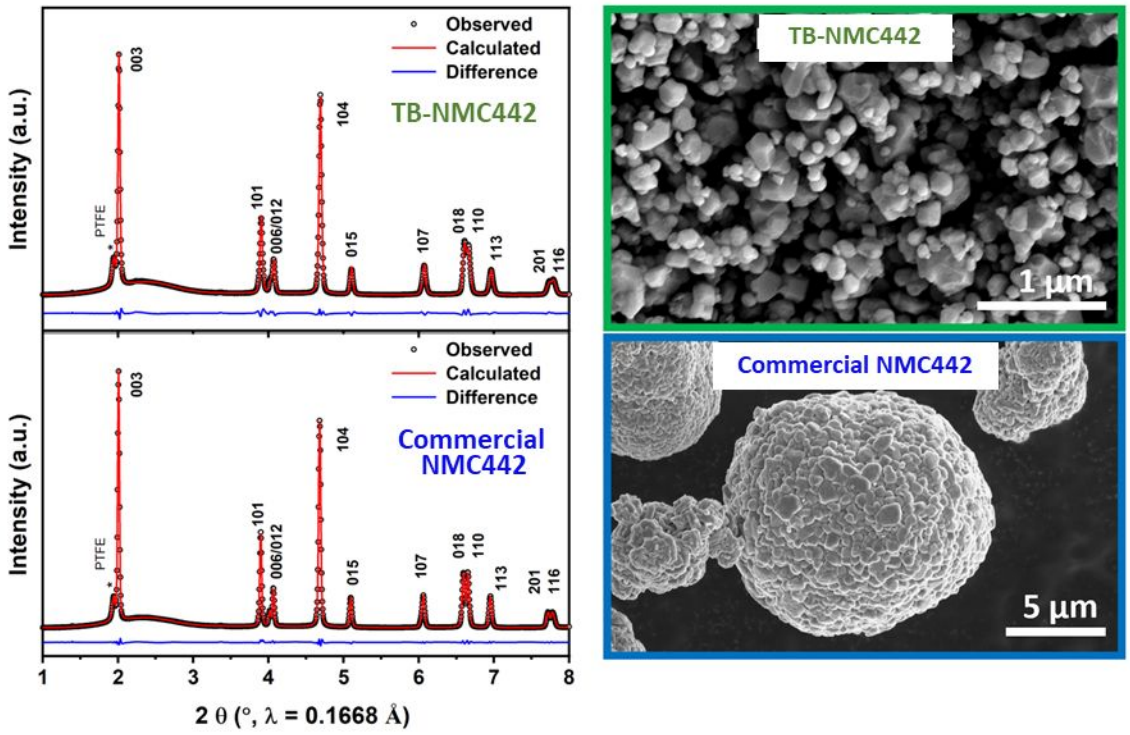

Figure S5. Rietveld refinements of high-resolution synchrotron XRD data and the corresponding morphology of the pristine electrode mixture prepared with TB-NMC442 (top, green) and commercial NMC442 (bottom, blue), respectively.

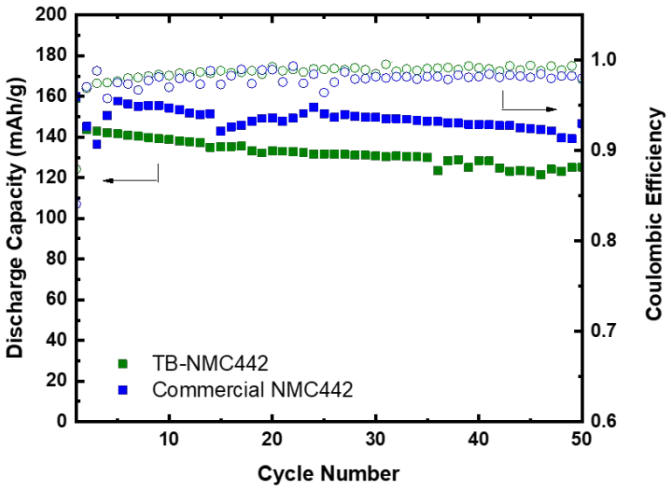

Figure S6. Cycling Performance of TB-NMC442 and commercial NMC442 in the voltage range of 2.5-4.3 V at C/10-rate.

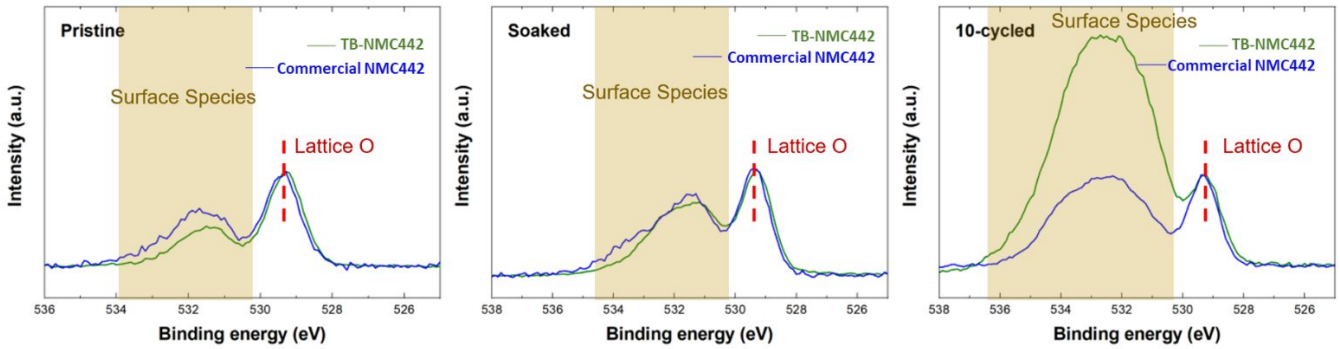

Figure S7. XPS result of the O 1s region for pristine, 6 h-electrolyte soaked, and 10-cycled TB-NMC442 and commercial NMC442 electrodes. The spectra were normalized to the lattice O peak to clearly visualize the relative peak intensity between the lattice O and surface species.

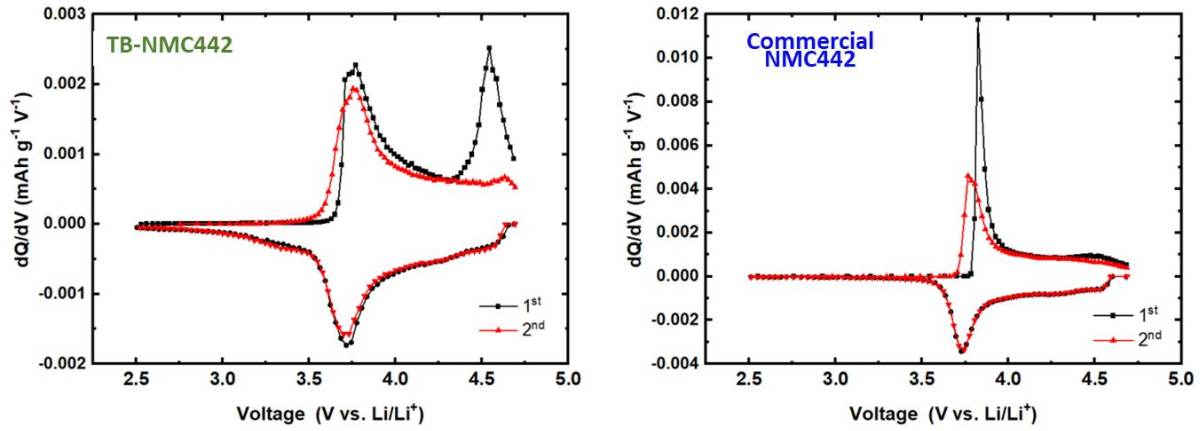

Figure S8. dQ/dV curves for the 1st and 2nd cycles of TB-NMC442 and commercial NMC442 (2.5-4.7 V).

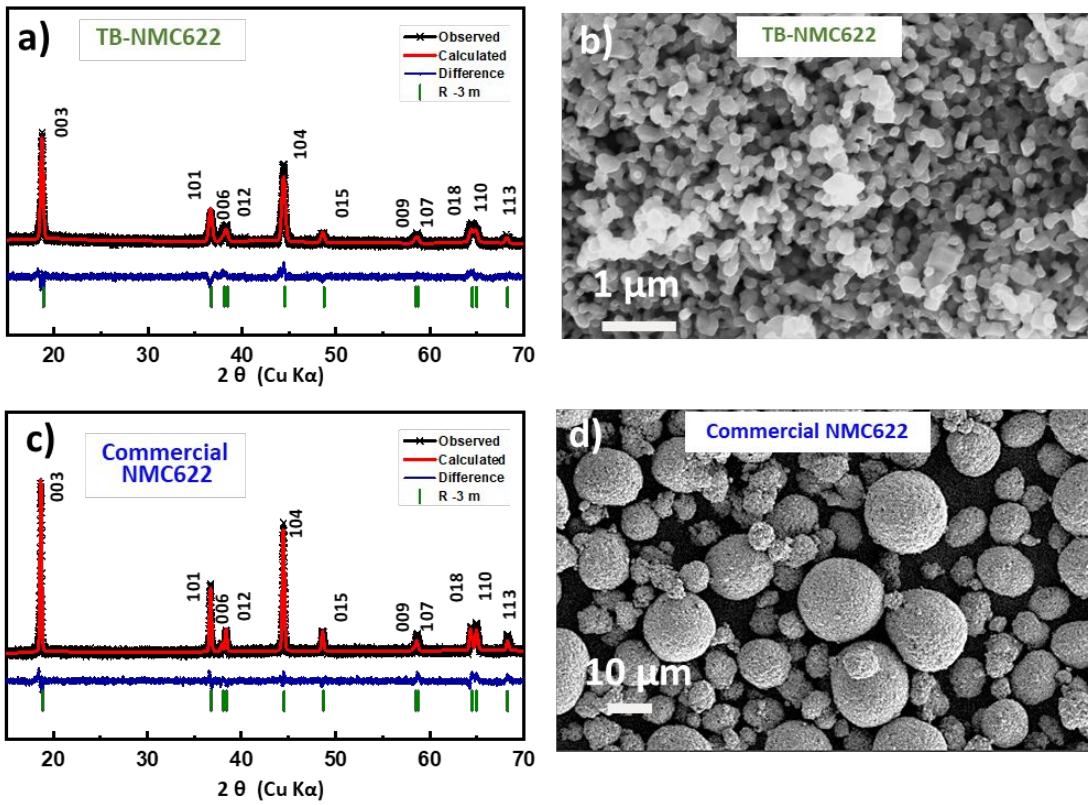

Figure S9. Rietveld refinements of XRD pattern and the corresponding morphology of the pristine NMC622 samples. a) and b) TB-NMC622; c) and d) commercial NMC622.

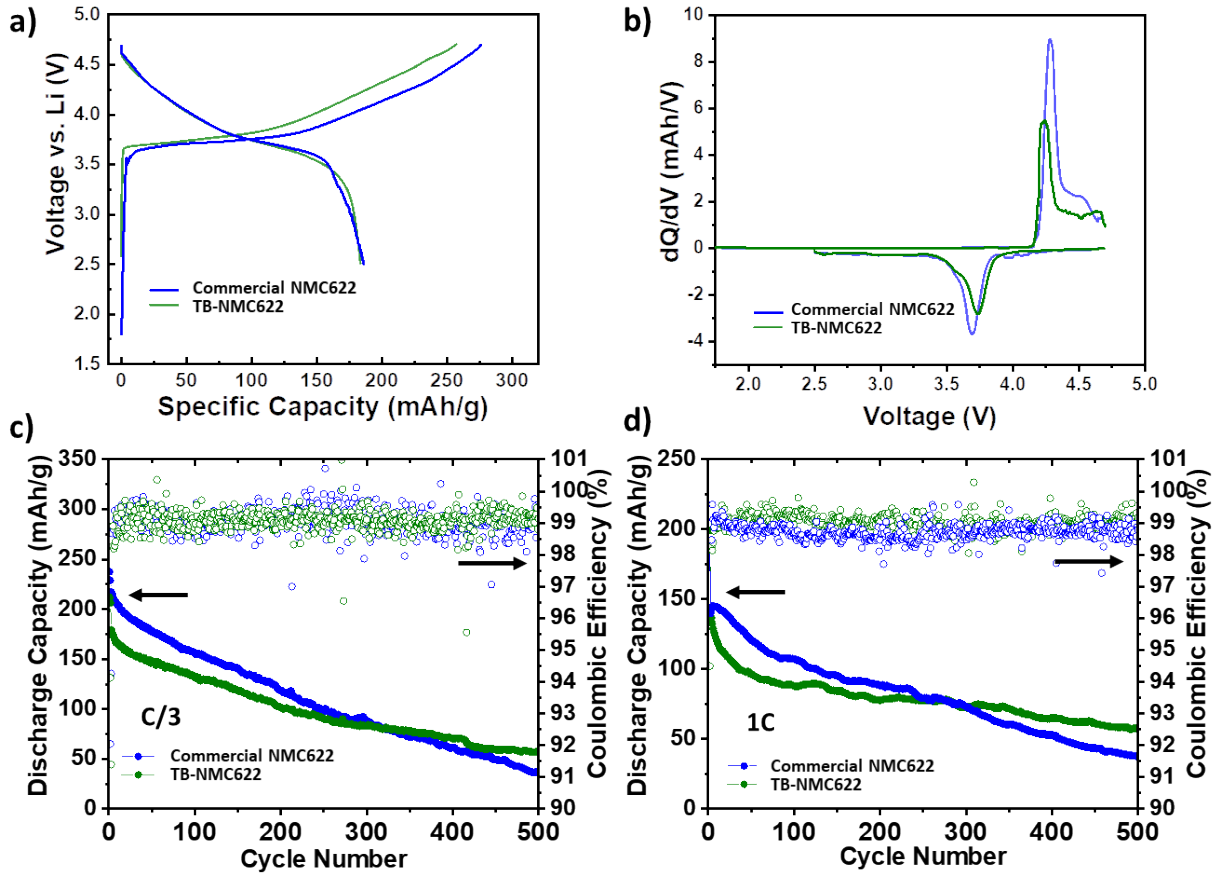

Figure S10. Electrochemistry performance of TB-NMC622 and commercial NMC622 in the voltage range of 2.5-4.7 V. a) the charge-discharge voltage profile of initial cycle at C/10-rate, cells continued with 1 C cycling as shown in figure c; b) dQ/dV plot of the initial cycle; c) capacity and Coulombic efficiency of NMC622 over 500 cycles at C/3-rate; d) capacity and Coulombic efficiency of NMC622 over 500 cycles at 1 C-rate.

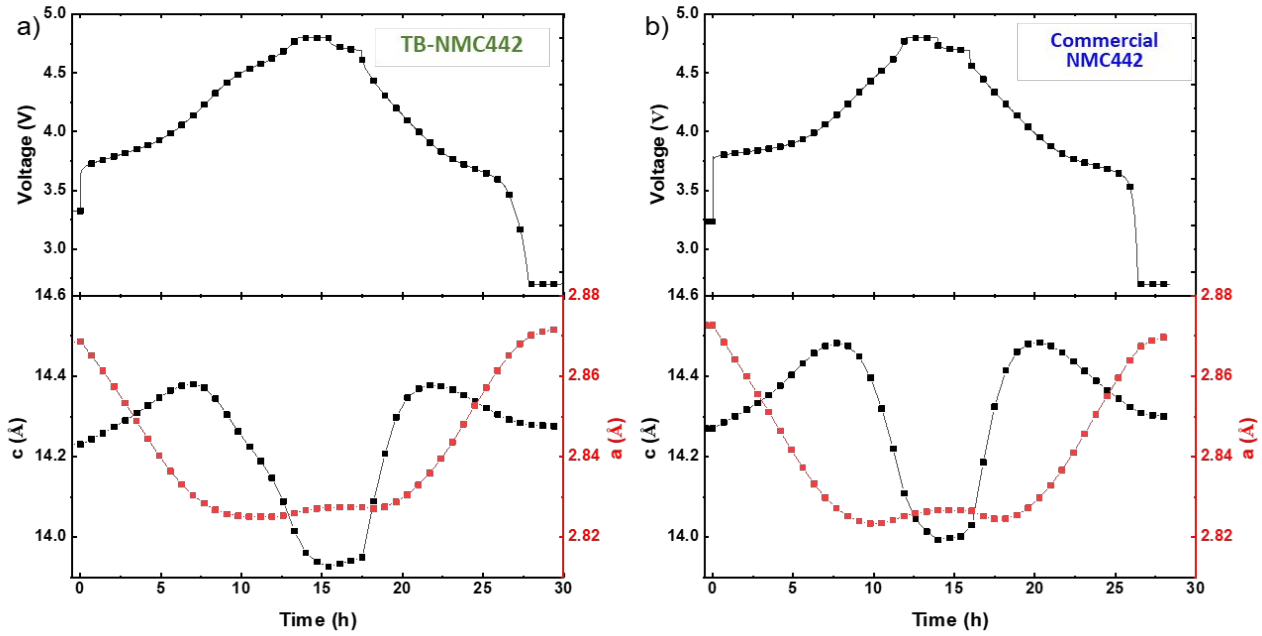

Figure S11. Electrochemical charge/discharge voltage profile with corresponding lattice parameters at different states of Li content for a) TB-NMC442 and b) commercial NMC442.

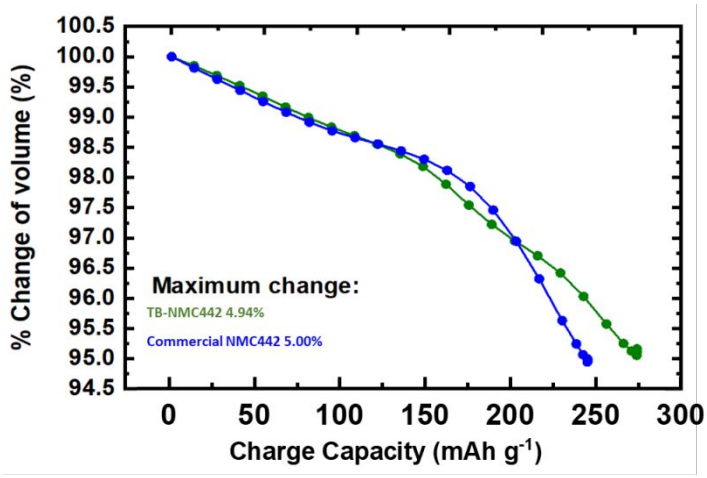

Figure S12. Comparison of the total volume change as a function of charge capacity during charge to 4.8V (followed by a 4.8 V hold for 2 h and a 2 h rest).

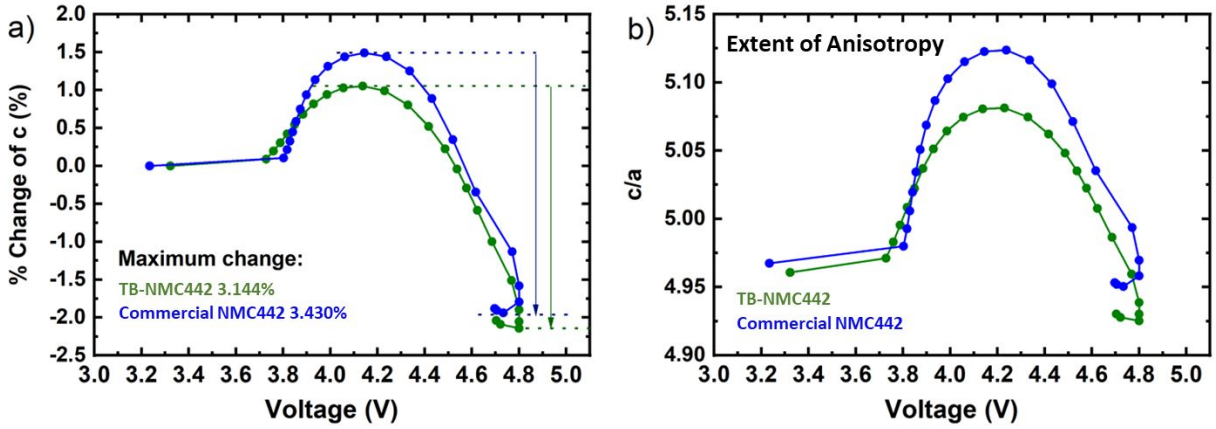

Figure S13. Comparison of the corresponding calculated lattice parameters along a) c-axis and b) the c/a ratio, showing the degree of anisotropy of the lattice changes as a function of voltage (vs. Li/Li$^+$) during charge to 4.8 V followed by 2 h hold at 4.8V and rest for 2 h.

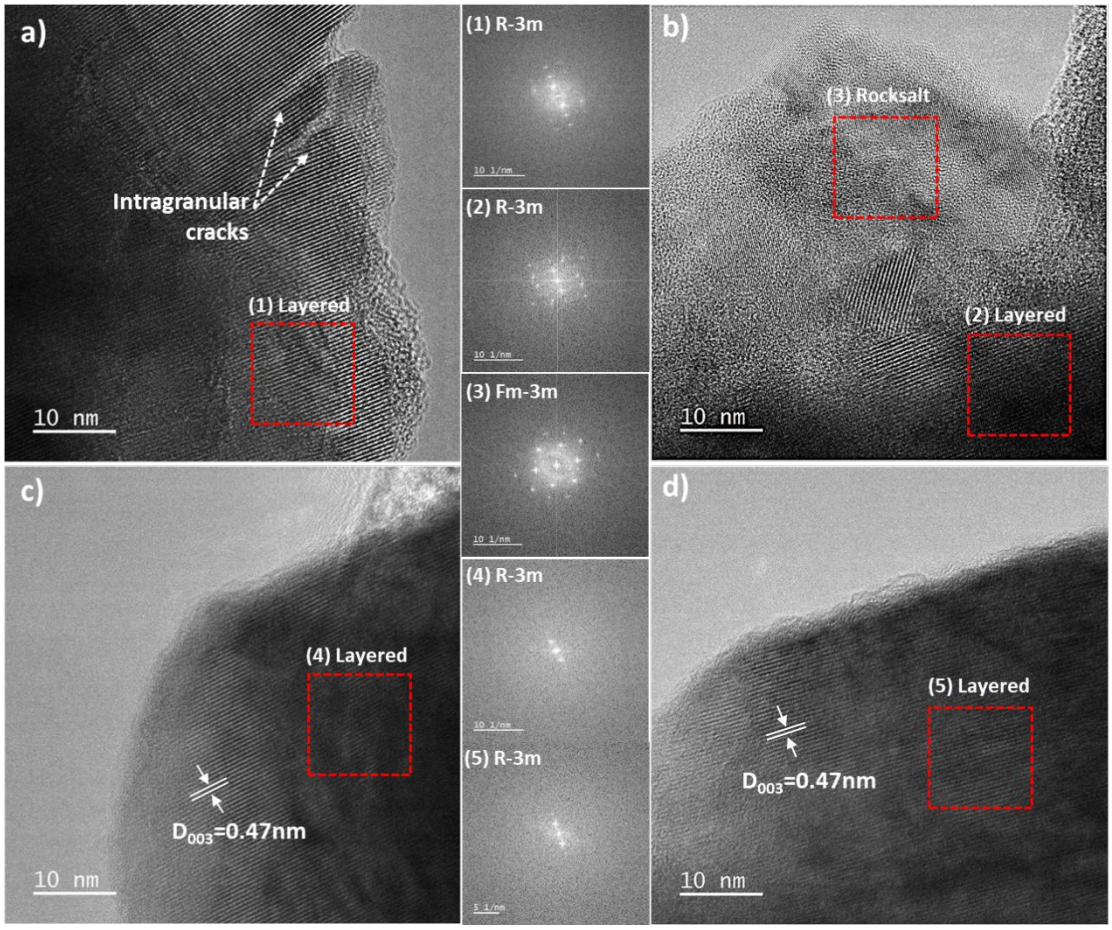

Figure S14. HR-TEM images of 500-cycled NMC materials. a) and b) commercial NMC622; c) and d) TB-NMC622.

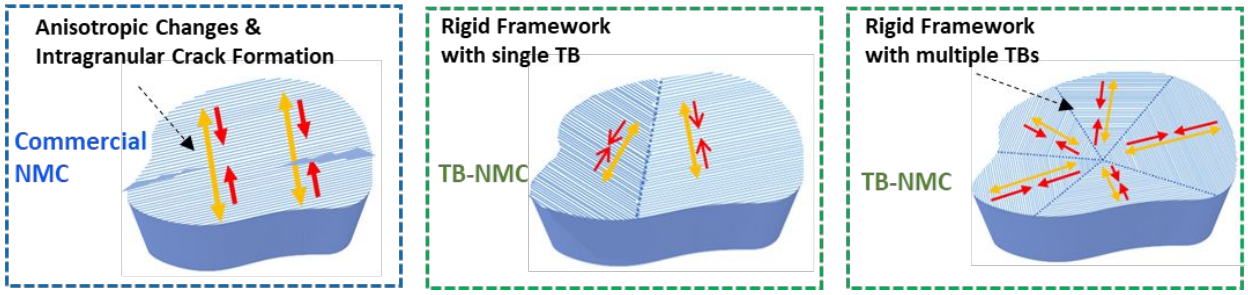

Figure S15. Schematics intragranular crack formation in commercial NMC and TB-NMC with different amounts of TB defects.

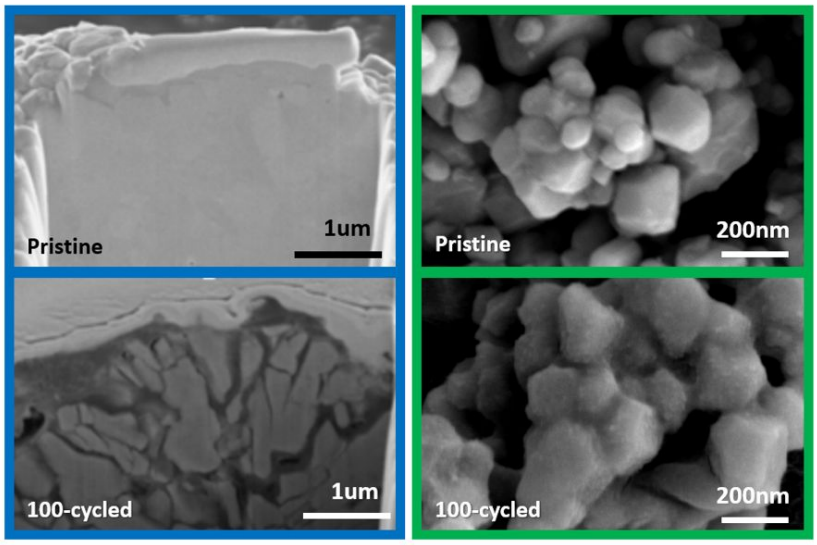

Figure S16. Cross sectional images of pristine and 100-cycled commercial NMC442 with higher magnification (blue frame). Pristine and 100-cycled TB-NMC442 prior to cutting with focused-ion beam (green frame).

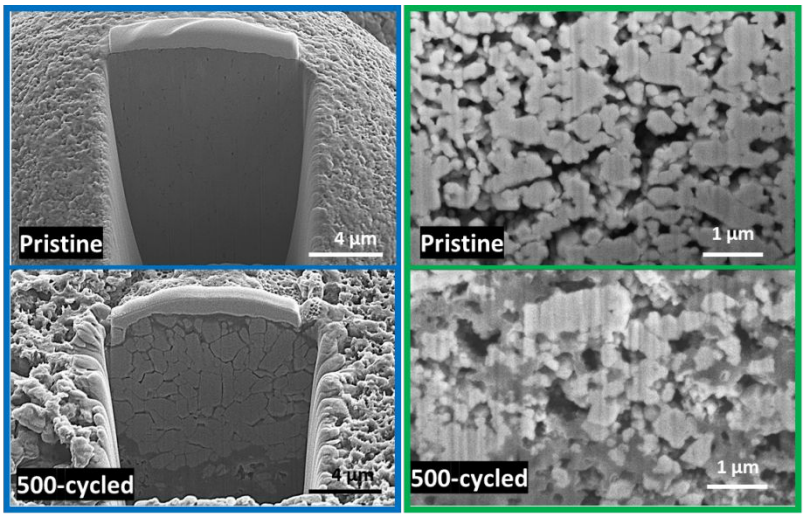

Figure S17. Cross sectional images of pristine and 500-cycled commercial NMC622 (blue frame) and TB-NMC622 (green frame).

Table S1. NMC/Li half cell coin cell testing specifications.

Active material	NMC – 80 %
Conductive agent	SPC65 – 10 %
Binder	HSV900 – 10 %
Counter electrode	Li metal chip (Thickness: 1 mm, diameter: 15.4 mm)
Separators	Celgard 2325
Electrolyte type	1M $LiPF_6$ in EC:DMC = 3:7 vol. %
Electrolyte amount	55 µl
Cell type	CR2032
Coin cell setup	0.5 mm-thick spacer and one spring at the anode side
Voltage range	2.5 - 4.7 V
Test protocols	Rest for 6 h after assembling, then 20 mA g^{-1} (C/10) for first 2 cycle, the rest cycling at 66.7 mA g^{-1} (C/3) or 200 mA g^{-1} (1C) at room temperature

Table S2. ICP-MS result of the NMC442 Cathode.

Sample	Ni : Mn : Co	Li : (Ni+Mn+Co)
TB-NMC442	0.400 : 0.400 : 0.200	1.008:1
Commercial NMC442	0.396 : 0.398 : 0.206	1.034:1

Table S3. ICP-MS result of the NMC622 Cathode.

Sample	Ni : Mn : Co	Li : (Ni+Mn+Co)
TB-NMC622	0.590 : 0.196 : 0.214	1.035:1
Commercial NMC622	0.610 : 0.198 : 0.193	1.062:1

Table S4. Lattice parameters, degree of Li/Ni cation mixing, and R factors from Rieveld refinement for NMC442 syncrotron XRD patterns.

Sample	TB-NMC442	Commercial NMC442
a = b (Å)	2.86868(4)	2.87265(2)
c (Å)	14.2304(3)	14.2692(1)
V (Å^3)	101.417(4)	101.975(2)
O *z* coord.	0.2589(1)	0.25841(6)
Ni-Li mixing	0.0566(8)	0.0510(5)
R_{wp} (%)	3.470	2.233

Table S5. Lattice parameters, degree of Li/Ni cation mixing, and R factors from Rietveld refinement for NMC622 XRD patterns.

Sample	TB-NMC442	Commercial NMC442
a = b (Å)	2.8704(3)	2.8692(3)
c (Å)	14.2301(2)	14.2407(2)
V (Å^3)	101.797 (1)	101.534(2)
O *z* coord.	0.2437(1)	0.2480(1)
Ni-Li mixing	0.053(3)	0.048(3)
R_{wp} (%)	1.957	2.807